ChemCatChem

Research Article
doi.org/10.1002/cctc.202500070

Chemistry Europe
European Chemical Societies Publishing

www.chemcatchem.org

Carbon-Based Bifunctional Lewis/Brønsted Acid Catalysts for 5-HMF Production from Cellobiose

A. Tonelli,[a] R. Tomer,[a] A. Morena,[b] L. Fusaro,[b] C. Aprile,[b] and S. Hermans*[a]

Bifunctional carbon-based acid catalysts presenting Brønsted and Lewis acid sites in different proportions were synthesized by grafting mesoporous aluminosilicate patches in coexistence with benzyl sulfonic moieties on the solid's surface. The final bifunctional systems were obtained by development of a methodology allowing the production of a model discontinuous silica layer on the carbon substrate before applying the optimized procedure to the desired alumino-silicate layer. Patches were necessary to expose bare carbon surfaces for sulfonic acid grafting employing a diazonium coupling methodology to ensure robust anchoring. The bifunctional solids and their monofunctional counterparts were fully characterized and their acidic nature, together with the presence of both Brønsted and Lewis acid sites, was assessed by Py-FTIR spectroscopy, NH_3-TPD, solid-state ^{31}P MAS NMR, and Boehm back titration. The attainment of a mesoporous discontinuous oxide framework was confirmed by nitrogen physisorption and SEM/TEM observations. Finally, the catalytic performance of both the produced bifunctional systems and their monofunctional counterparts was investigated and compared for the upgrading of cellobiose to 5-hydroxymethylfurfural (5-HMF). A maximal yield of 37% of 5-HMF out of a 96% of cellobiose conversion was attained after 23 h with catalyst I4@BATEOS/SO_3H in a designed solvent mixture (THF:mQ water) at 423 K.

1. Introduction

With the diminishing of fossil resources, the development of new technologies to exploit versatile and renewable biomasses as alternative feedstock for platform chemicals has received more attention than ever.[1] In this scenario, because of its abundance, lignocellulosic biomass has shown much promise as a valid sustainable resource.[2–4] In essence, lignocellulosic biomass is a complex bio-based substance made of cellulose (30–50 wt%), hemicellulose (20–40 wt%), and lignin (10–20 wt%).[1] Cellulose is a polymer of glucose with varying degrees of polymerization; hemicellulose is a heteropolymer of pentose and glucose linked by β-1, 4- glycosidic bonds; lignin mainly consists of amorphous aromatic macromolecules.[5–7] One of the possible products derived from the major component of lignocellulosic biomass, i.e., cellulose, is 5-hydroxymethylfurfural (5-HMF). It is a high added-value chemical and has been included among the "top 10 + 4" bio-based key platform compounds by the U.S. Department of Energy.[1] In fact, the oxidation/reduction of 5-HMF can yield valuable industrial chemicals such as 2, 5-furandicarboxylic acid (FDCA), 5-hydroxymethyl-2- furancarboxylic acid (HMFCA), 5-formyl-2-furancarboxylic acid (FFCA), 2, 5-diformylfuran (DFF), 2, 5-bis(aminomethyl)furan (BAMF), (tetrahydrofuran-2, 5-diyl)dimethanol (THFDM), 2, 5-dimethyl furan (DMF), and 5-methylfuran-2-carbaldehyde (MFC).[8,9] These upgraded platform chemicals can be applied in various fields, including biofuels and fuel additives production, plastics and packaging, pharmaceuticals, and many more.[10]

Concerning 5-HMF production, it can be directly sourced from cellulose, following a three-step catalytic conversion process (Scheme 1). First, the hydrolysis of cellulose to glucose, catalysed by Brønsted acid sites (BA), occurs, directly followed by the isomerization of the attained glucose into fructose, mediated this time by Lewis acid moieties (LA). Finally, the dehydration of fructose to 5-HMF is achieved, facilitated again by Brønsted acid sites. During the conversion, various side reactions might occur and reduce the final 5-HMF yield, including rehydration of the latter to levulinic acid and formic acid, and cross-polymerization to humins via direct sugars degradation or other intermediates.[11] Taking all these challenges into account, the Brønsted-Lewis acidity ratio in the catalyst plays a crucial role in directing the conversion process toward a selective production of 5-HMF.

Catalysis is an effective strategy for producing refined industrial chemicals from a biomass feedstock, because it lowers the activation energy required and promotes both conversion and selectivity, improving the overall reaction conditions.[12,13] In the valorisation of cellulose to 5-HMF, various homogeneous acid catalysts such as mineral salts (i.e., $AlCl_3$, $FeCl_3$, $RuCl_3$, VCl_3, $TiCl_3$, $MoCl_3$, and $CrCl_3$)[14] or acids (HCl and H_2SO_4 mainly) have been used to overcome the resistance to degradation of cellulose.[1] However, serious drawbacks have been associated to the use of such catalysts in terms of difficult product separation, corrosion hazard, waste fluids treatment, and the often-required severe operative conditions.[15,16] Furthermore, classical homogeneous catalysts are not easily tuneable in terms of properties of their acid sites, such as strength, density on the surface, and the

[a] A. Tonelli, R. Tomer, S. Hermans
Université catholique de Louvain, Institute of Condensed Matter and Nanosciences (IMCN), Place L. Pasteur 1, Louvain-la-Neuve 1348, Belgium
E-mail: sophie.hermans@uclouvain.be

[b] A. Morena, L. Fusaro, C. Aprile
Laboratory of Applied Materials Chemistry, Unit of Nanomaterials Chemistry, Chemistry Department, NISM, University of Namur, Rue de Bruxelles, Namur 61,5000, Belgium

Supporting information for this article is available on the WWW under https://doi.org/10.1002/cctc.202500070

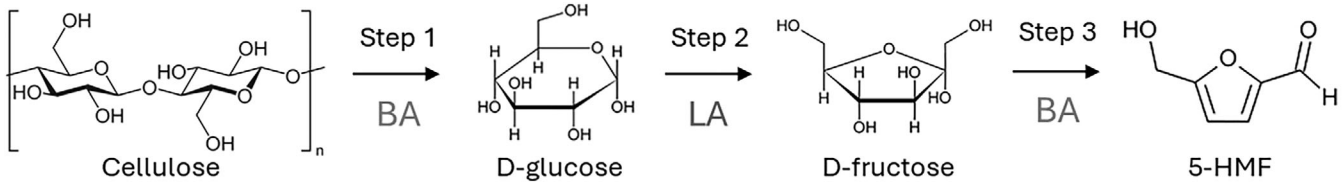

Scheme 1. Synthesis of 5-hydroxymethylfurfural (5-HMF) from cellulose; 3 steps cascade process involving Brønsted (BA) and Lewis (LA) acid sites.

possibility to combine both Brønsted and Lewis moieties. Compared to homogeneous systems, heterogeneous acid catalysts show many merits in terms of efficient conversion and selectivity, flexible separation and easy recycling, and low toxicity, thus making them more interesting for industrial applications.[17–19] Therefore, some novel solids with Brønsted and/or Lewis acidic sites, such as carbon-based supports,[20–22] resins,[23] heteropoly acids,[24,25] and zeolites[26,27] have been explored for 5-HMF production from various feedstocks, i.e., glucose, fructose, and cellulose. These catalytic systems can be cleverly designed with an appropriate combination of Brønsted (B) and Lewis (L) acid sites. However, the best balance between B/L acidity is not fully understood, and the stability of heterogeneous catalysts in presence of water (generated during the process) or other impurities represents a further challenge. In addition, these systems also suffer from deactivation problems like poisoning or leaching of the active sites.[28] Alongside, the porosity of the selected catalyst also plays a key role in the conversion of biomass to 5-HMF, which is favorably attained in the presence of mesopores that can facilitate the interaction between the bulky sugary feedstock and the available active sites. These mesopores can be easily introduced in the material when dealing with metal-oxides thanks to the use of a templating agent, such as cetrimonium bromide (CTAB).[30]

Given the highly oxygenated nature of biomass, carbon-based catalysts are among the best possible systems, because they can more easily sustain water and O-rich media than other supports, in combination with good mechanical and chemical resistance under the required conditions (high temperature, pressure, designed solvents, extreme pHs, etc.).[44] Furthermore, a carbon-based substrate offers a better cost-effective alternative to other possible potential supports, while also providing the advantages of its various available forms, including carbon black, activated carbon powders or nanostructures (graphene sheets, nanotubes, etc.). Such a support is also easily functionalized, with controlled and tuneable features, thus helping to overcome some of the main aforementioned difficulties.[44] Therefore, the main emphasis of this work is on synthesizing a novel catalytic system consisting of a carbon-based support functionalized with both Brønsted and Lewis acid moieties. Sulfonated carbons were explored as Brønsted acidity contributors,[36] while a methodology for the growth of a discontinuous metal-oxide layer at the carbon substrate's surface for acquiring the desired Lewis acidity was developed. As a last step, the two moieties were combined to produce the final bifunctional catalysts by varying the Brønsted/Lewis acidity ratio introduced in order to assess the impact of this role-playing feature on their activity for the direct conversion of cellobiose into 5-HMF. The hydro-soluble disaccharide was specifically chosen as a model molecule for cellulose to overcome any initial insolubility issue and complex decomposition behavior.[11] The reaction was carried out in a solvent mixture consisting of THF and milliQ water to prevent further rehydration of 5-HMF and to easily recover the immiscible catalysts. The proximity effect of the two acid functionalities introduced was also investigated in order to confirm whether an actual improvement was brought to the catalytic performance. Specific tests were conducted to compare the outcome attained when a mixture of the two mono-functional catalysts (sulfonated carbon and metal-oxide patched carbon) is used instead of the designed bifunctional system.

2. Experimental Section

2.1. Reagents and Materials

The activated carbon (SX^+, fraction <50 µm only was kept by sieving) was obtained from NORIT, while the carbon black support (CB, 250 G type) was received from IMERYS GRAPHITE & CARBON. Hexadecyltrimethylammonium bromide (CTAB, 95%), (3-aminopropyl)trimethoxysilane (APTES, 99%), tetraethyl orthosilicate (TEOS, >98%), thionyl chloride ($SOCl_2$, >99%), sulfanilic acid (99%), isopentyl nitrite (96%), and D-(+)-cellobiose (≥99%), were purchased from Sigma Aldrich and used as received. Bis(sec-butoxy)aluminoxytriethoxysilane $[(sec\text{-}BuO)_2AlOSi(OEt)_3]$ (BATEOS) was purchased from Alfa Aesar. A commercial ultrasonic cleaner (VWR) was used for sonication.

2.2. Methods

2.2.1. Synthesis of the Sulfonated Carbons

The functionalization of the carbon substrates (SX^+, CB) with benzyl sulfonic groups was carried out by means of a diazonium coupling method.[29] In this procedure, 1 g of carbon solid was dispersed in 60 mL of distilled water in a round bottom flask. Subsequently, 1.5 g of sulfanilic acid were added and the suspension was stirred at 343 K for 10 min. After cooling down the system to 303 K, 1.2 mL of isopentyl nitrite was added and the mixture was stirred during 16 h at the same temperature. The solid was then filtered out and washed with distilled water and ethanol. The resulting material was dried overnight at 273 K under atmospheric pressure.

2.2.2. Synthesis of a Discontinuous Silica Layer

Discontinuous mesoporous silica patches at the surface of the carbon substrates were attained by modification of a precedent methodology developed by *Haynes* et al.[30] Different trials (T0, T1, T2, T3, and T4, as shown in Table 1), were synthesized to understand the effect of the gradual decrement of the precursors' amount on

Table 1. Amounts of precursors introduced for the synthesis of the different trials of silica patches on carbon.

Entry	$SOCl_2$ (mL)	APTES (mL)	TEOS (mL)	CTAB (mg)
T0	4.2	0.71	0.5	400
T1	3.4	0.57	0.4	325
T2	2.6	0.43	0.3	245
T3	1.7	0.28	0.2	162
T4	0.86	0.14	0.1	82

the growth of the oxide layer. The reciprocal molar ratios of all reactants involved were kept as optimized.[30] The whole methodology consists of three different steps, necessary to ensure the final bonding of the silica oxide onto the carbonaceous substrate, avoiding the formation of nongrafted isolated SiO_2 bodies.

In the synthesis of T0 (Table 1), 2 g of carbon solid (CB or SX^+) was introduced in a 250 mL round-bottom flask containing 100 mL of toluene. After addition of 4.2 mL of $SOCl_2$, to activate the O-groups (Cl^- being a better leaving group than OH^-), the mixture was refluxed at 393 K for 5 h. The solid was then filtered out and washed with toluene (150 mL). The resulting material (carbon-Cl) was dried overnight at 273 K. For the subsequent step, 1 g of carbon-Cl was introduced in a 250 mL round-bottom flask containing 100 mL of dichloromethane. 0.71 mL of APTES were added, and the mixture was stirred for 24 h at room temperature. The material (carbon-APTES) was filtered out, washed with dichloromethane (100 mL) and methanol (100 mL) followed by drying overnight at 273 K. The functionalization by APTES allows to direct the subsequent growth of the silica layer onto the carbon surface to coat it, preventing the formation of separated silica particles. Finally, 0.250 g of carbon-APTES were introduced in a 100 mL round bottom flask containing 25 mL of distilled water. Then, 10 mL of NaOH (0.1 M) were added to facilitate the sol-gel process and the mixture was sonicated 10 min. Further, 0.4 g of CTAB were added to this suspension for the production of mesopores in the final silica layer and the resulted solution was heated at 333 K. Once the desired temperature was reached, 0.5 mL of TEOS were added dropwise within 30 min. The suspension was further stirred for 3.5 h, then charged into a propylene bottle which was tightly closed and heated at 373 K for 3 days. The final product was filtered out, washed with ethanol (100 mL) and afterward dried at 373 K overnight. Finally, the CTAB template was removed by refluxing in ethanol for 24 h. The other trials T1, T2, T3, and T4 were synthesized by the same methodology as above, but accordingly gradually diminishing the amounts of precursors as reported in Table 1. The quantity of starting carbon material was kept unaltered in each step.

2.2.3. Synthesis of the Bifunctional Catalysts

To produce the final bifunctional material, the conditions of choice to be adapted to the use of a mixed Al-Si precursor (Scheme 2), namely bis(sec-butoxy)aluminoxytriethoxysilane,[31] were those of either a maximal (T0, Table 1) or a minimal (T4, Table 1) quantity of oxide introduced in the trials to obtain a discontinuous silica layer. These were named catalyst I0 (produced by applying T0 conditions) and I4 (produced by applying T4 conditions), where the letter *I* is used to indicate the presence of metal-oxide islands on the sample.

To prepare the carbon-APTES precursor, the same methodology as described in § 2.2.2 was followed. To synthesize the discontinuous mesoporous Lewis acid layer, 0.250 g of carbon-APTES were added to a 100 mL round bottom flask containing 40 mL of ethanol. Subsequently, 1.4 g of CTAB (0.270 g in case of I4) was introduced for the production of mesopores in the final aluminosilicate layer. Finally, 0.8 mL of BATEOS (0.2 mL for I4) were added and the mixture was stirred for 1 h at room temperature. To this suspension, 40 mL of water were added dropwise within 4 h, after which the solution was charged into a propylene bottle and heated at 273 K for 3 days. The product was filtered out, washed with ethanol (50 mL) and dried at 273 K overnight. Lastly, the CTAB template was removed by refluxing the solid in ethanol for 24 h.

Finally, to synthesize the desired bifunctional system, the patched materials were functionalized with benzyl sulfonic moieties (Figure 1) as described in §2.2.1. In addition, to unveil the impact the order of applied steps might have upon the properties of the materials, catalysts I0 and I4 were resynthesized by inverting the methodology described and grafting the sulfonic groups before growing the metal-oxide patches.

All the obtained samples will be specified by their entry name followed by @ and the acronyms of the introduced moieties: SiO_2 and BATEOS for the metal oxides, SO_3H for the benzyl sulfonic groups (for instance T0@SiO_2 in the case of carbon coated with silica patches by following T0 preparation (Table 1), or I0@BATEOS/SO_3H for samples coated with aluminosilicate islands and grafted with benzyl sulfonic moieties by following the procedure reported in §2.2.3). For every specimen, the substrate used will be specified with the acronyms CB in the case of carbon black, and SX^+ as for activated carbon powder.

2.3. Characterizations

The solid catalysts were characterized by transmission/scanning electron microscopy (TEM/SEM), photoelectron spectroscopy (XPS), elemental analyses (ICP, microgravimetry and EDX), N_2-physisorption, Py-FTIR spectroscopy, NH_3 TPD, solid-state ^{31}P MAS NMR, and Boehm titration.

TEM images were obtained on a LEO 922 Omega Energy Filter Transmission Electron Microscope operating at 120 kV. The samples were suspended in dichloromethane under ultrasonic treatment. A drop of the suspension was deposited on a holey carbon film supported on a copper grid (Holey Carbon Film 300 Mesh Cu, Electron Microscopy Sciences), which was dried at room temperature before introduction in the microscope.

SEM images were obtained on a JEOL 7600F Field-Emission Scanning Electron Microscope operating at 15.0 kV. The samples were prepared by placing the powders on a double-faced copper tape supported onto a thin aluminum lamina. The applied probe current was set at 12 A for direct imaging on powders, and at 16 A in case of Energy Dispersive X-ray Spectroscopy (EDX) probing (that was used for semi-quantitative elemental analyses for C, O, Si, Al, S, qualification as average of three different points). The analytical accuracy of the performed EDX probing is ±2%.

XPS analyses were carried out at room temperature with a SSI-Xprobe (SSX 100/206) photoelectron spectrometer from Surface Science Instruments (USA), equipped with a monochromatized microfocus Al X-ray source. Samples were stuck onto small sample holders with double face adhesive tape, then placed on an insulating ceramic carousel (Macor, Switzerland). Charge effects were avoided by placing a nickel grid above the samples and using a flood gun set at 8 eV. The binding energies were calculated with respect to the C-(C, H) component of the C1s peak fixed at 284.8 eV. Data treatment was performed using the CasaXPS program (Casa Software Ltd., UK) and the peak assignment was done thanks to the *xpsdatabase.net* database. The peaks were decomposed into a sum of Gaussian/Lorentzian (85/15) after subtraction of a Shirley-type baseline and using sensitivity factors provided by the manufacturer. The analytical accuracy of the performed XPS probing is ±10%.

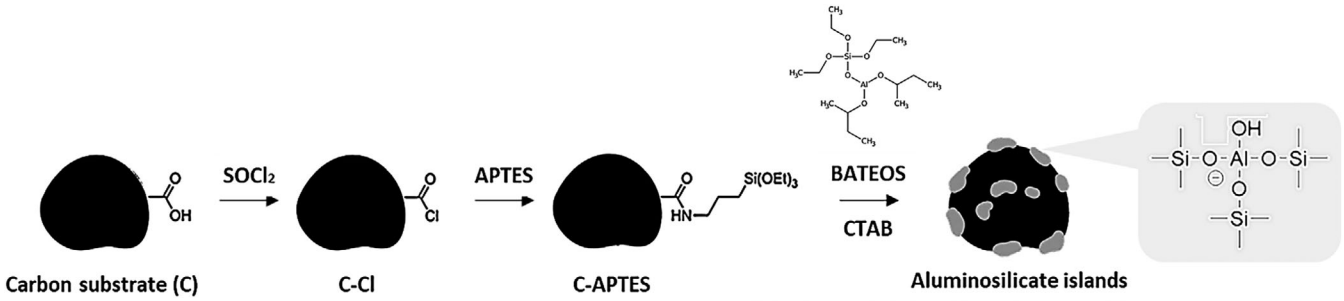

Scheme 2. Synthesis of the mixed metal oxide patches from a single aluminosilicate precursor BATEOS (Al/Si = 1).

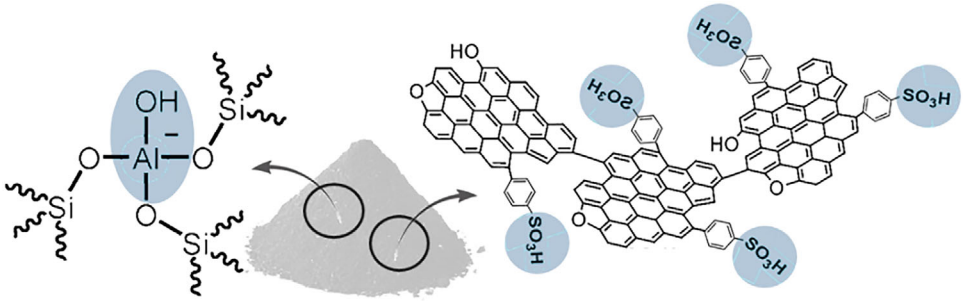

Figure 1. Schematic overview of the final bifunctional systems functionalized with both aluminosilicate patches and benzyl sulfonic moieties (—SO_3H).

The elemental quantification was performed by MEDAC Ltd. (UK). Al and Si were analyzed by Inductively Coupled Plasma (ICP) Spectroscopy with a Varian 720ES instrument after acid digestion (HF and H_2SO_4) of the sample. C, H, N, and S were detected by microgravimetry with a FlashEA 1112 Elemental Analyzer.

The pore texture of the catalysts was characterized by nitrogen physisorption isotherms. The measures were achieved by using a Micromeritics ASAP 2020 analyzer at 77 K. Before analysis, the samples (0.02–0.10 g) were degassed for 2 h at 373 K with a heating rate of 10 K min^{-1} under 10^{-3} bar pressure. The analysis of the isotherms provided specific surface areas (S_{BET}) calculated with the Brunauer–Emmett–Teller (BET) equation. The pore volume, V_p, of the samples and the pores average diameters were calculated using the Barrett–Joyner–Halenda (BJH) model on the desorption branch.

Acidity measurements were performed by pyridine-FTIR (Py-FTIR), temperature-programmed desorption of ammonia (NH_3—TPD), and solid-state nuclear magnetic resonance of 31 P with trimethylphosphine as probe molecule (^{31}P MAS NMR). Py-FTIR was conducted to identify Lewis and Brønsted acidic sites on the pure oxide frameworks, following a methodology similar to our previous work.[40] In a typical experiment, the synthesized catalysts (50 mg) were dried under vacuum at 393 K for 1 h and then cooled down to room temperature under vacuum. Approximately 10 mg of the dried sample was soaked in 0.1 mL of Pyridine for 1 h to ensure the complete adsorption of the molecule. The Pyridine-adsorbed sample was subsequently dried at 393 K for 1 h to remove the excess Pyridine. The prepared samples (1 mg) were then mixed with KBr (99 mg) and pelletized using a manual hydraulic press. The FT-IR spectra of pellets were taken in transmission mode using a spectrometer IFS55 Equinox (Bruker) equipped with a DTGS detector. The spectra were recorded with 100 scans between 400 and 4000 cm^{-1}.

The total acidity was measured by using temperature-programmed desorption (TPD) with ammonia as the probe molecule, employing a Hiden Catlab gas analyzer coupled with a QGA Hiden quadrupole mass spectrometer. Before analysis, the catalyst sample (20–30 mg) was degassed at 473 K for 1 h under an Argon flow of 30 mL min^{-1}. Subsequently, NH_3 adsorption was carried out at 333 K for 1 h using a gas mixture of Argon and 5% NH_3-He, at a flow rate of 15 mL min^{-1} each. Ammonia desorption was then recorded under an Ar flow of 30 mL min^{-1}, as the temperature was increased from 333 to 823 K at a rate of 10 K min^{-1}. The total acidity was calculated based on the integral area of the peaks corresponding to the desorbed molecules versus the desorption temperature curve.

Boehm back titration method was used to evaluate the total acidity of carbon-based catalysts.[32,33] A 0.05 M NaOH solution was prepared from a concentrated (1 M) sodium hydroxide standard (Sigma Aldrich). The HCl solution was produced by dilution of a concentrated hydrochloric acid (37%, VWR Chemicals) and its exact concentration was determined by titration with the standard NaOH. These solutions were prepared with mQ water and were decarbonated by a 2 h Argon degassing. For titrating the acid groups, 25 mg of sample were dispersed in 25 mL of NaOH 0.05 M and the solution was decarbonized for 1 h under Ar flux. The mixture was then agitated for 23 h under Ar atmosphere, after which the suspension was filtrated. A 20 mL of HCl 0.05 M were added to 10 mL of the resulting filtrate and the solution was then degassed under Ar for 2 h before back titrating it with NaOH 0.05 M. The indicator used was phenolphthalein. The amount of acid functions on the catalyst was determined by calculating the difference between the initial amount of NaOH and the amount of NaOH titrated by the HCl using the following formula:

$$\text{Total acidity} = \frac{\frac{n_{HCl}}{n_{NaOH}}\left[(V_{NaOH} \times [NaOH]) - (V_{HCl} \times [HCl]) - V_t \times [NaOH_t] \times V_{NaOH}/V_s\right]}{W} \quad (1)$$

where V_t and $[NaOH_t]$ indicate the volume and concentration of titrating base, V_s is the volume of the basified aliquot, n_{HCl}/n_{NaOH}

refers to the molar ratio of HCl and NaOH, and *W* is the weight of the carbon catalyst employed.

^{31}P ss-NMR spectra were recorded at room temperature using a 400 MHz Varian VNMRS spectrometer equipped with a 4 mm Varian/Chemagnetics T3 probe. The instrument operated at 9.4 T (161.9 MHz for ^{31}P) with a spinning frequency of 8 kHz. Samples were packed in 4 mm Bio-solids cavern rotors provided by Phoenix NMR and sealed with nonvented PCTFE top spacers featuring two O-rings. The reported analysis is qualitative, and the experimental parameters included a $\pi/2$ pulse duration of 3.4 µs, a relaxation delay of 6 s, an acquisition time of 20 ms, and a total of 10,000 scans. Chemical shifts were externally referenced to ammonium dihydrogen phosphate ($(NH_4)H_2PO4$) with ^{31}P at 0.81 ppm.[34] A portion of the sample underwent a two-step dehydration process (details provided in Figure S16, Supporting Information). The 4 mm rotor was packed with the solid sample under an inert argon atmosphere inside a glovebox. Subsequently, 2 µL of liquid-phase trimethylphosphine (TMP) was added directly to the sample within the rotor. Excess TMP was removed by applying a vacuum of 10^{-6} mbar for 1.5 h at 100 °C using a custom-built setup, as described in the literature.[35]

2.4. Catalytic Tests

The catalytic activity tests were carried out in a 250 mL stainless-steel high-pressure Parr autoclave. In a typical experiment, 1 g of cellobiose was added to 0.5 g of catalyst in 120 mL of mQ water (for testing of the sulfonated substrates), or 120 mL of solvent mixture (90 mL of THF and 30 mL of mQ water) for testing the bifunctional materials. Then, the autoclave was sealed, and the system was purged three times with nitrogen and heated up to the desired temperature (413 K for testing the sulfonated substrates and 423 K for testing the bifunctional materials and their monofunctional counterparts) under 4.7 bar of nitrogen pressure. Finally, the agitation was started at 1700 rpm and the test conducted for 4 h. The system was then cooled down to room temperature and the solution was filtrated. The filtrate was then diluted to 250 mL with mQ water and analyzed by high-performance liquid chromatography (HPLC). The solid catalyst was thoroughly washed with mQ water and dried overnight at 373 K under atmospheric pressure. The catalysts recovered after a catalytic test will be indicated with R- before their acronyms.

Some blanks were also tested, such as the pristine carbon substrates CB and SX^+, pure SiO_2 and aluminosilicate oxide, and possible intermediates solids and monofunctional catalysts: (e.g., $(SX^+)@SO_3H$, $T0@SiO_2$, $T0@SiO_2/SO_3H$, $T4@SiO_2$, $T4@SiO_2/SO_3H$, I0@BATEOS, and I4@BATEOS). After test, the materials recovered were also noted with R- before their code names.

Moreover, a kinetic study was carried out for catalyst $I4@BATEOS/SO_3H$ in the biphasic environment at 423 K by sampling 1 mL aliquot every 2 h within the first 8 h, then collecting one last fraction after 23 h. Each aliquot was then diluted to 10 mL with mQ water and analyzed by HPLC.

The formed products were quantified by HPLC. Reaction mixtures arising from the conversion of cellobiose to glucose were analyzed through a Waters system equipped with a 2414 refractive index detector (RID, Waters, USA), while biphasic reaction mixtures (conversion of cellobiose to 5-HMF) were studied through an Agilent 1200 series system (Germany) equipped with a Diode Array Detector (DAD) (G1315D, Agilent) in series with a RID detector (G1362A, Agilent). In both cases, the same column, Aminex HPX87-H+ (Bio-Rad, USA) was used working with H_2SO_4 0.005 M as eluent, a flux of 0.55 mL min^{-1}, and 20 µL of injected volume. The temperature of column and RID were maintained at 338 and 323 K, respectively.

The cellobiose conversion was calculated as follows:

$$\text{Cellobiose conversion (\%)} = \frac{n \text{ cellobiose after reaction}}{n \text{ initial cellobiose}} \times 100 \quad (2)$$

The yield in the different products obtained was calculated as follows:

$$\text{Product yield (\%)} = \frac{n \text{ product obtained}}{2 \times n \text{ initial cellobiose}} \times 100 \quad (3)$$

3. Results and Discussion

3.1. Methodology Development

Two different carbon solids as substrates, namely activated carbon (SX^+) and carbon black (CB), were engaged in initial experiments with the aim of identifying the most suitable one for the preparation of the desired bifunctional materials. To understand the influence of the different available specific surface areas and morphologies involved, benzyl sulfonic grafting was first considered for both chosen substrates.

While CB particles present as expected the shape of regular small spheres (Figure 2A), SX^+ showed a nonuniform granular morphology and a general larger particles size compared to carbon black (Figure 2B). After diazonium coupling reaction to graft sulfonic acid groups, SEM imaging showed no structural changes in the substrates (Figure 2C,D).

The EDX elemental analysis performed (Figure S3, Supporting Information) instead revealed an average of 3% sulfur (atomic percentage) on the surface of activated carbon SX^+, a significantly higher value than the 0.21% detected for carbon black. The data above can be better contextualized by taking into consideration the BET surface area found for the two pristine substrates: with 913 m^2 g^{-1}, SX^+ is bringing about a higher surface for the grafting of $-SO_3H$ groups if compared to the 63 m^2 g^{-1} found for CB, therefore resulting in the observed higher functionalization.

Given the Brønsted acidity provided by the benzyl sulfonic moieties introduced, the obtained systems $CB@SO_3H$ and $(SX^+)@SO_3H$ were tested for catalytic activity by performing the hydrolysis of cellobiose into D-glucose. This first step for the production of 5-HMF, driven by Brønsted acidity, was carried out under nitrogen pressure in pure mQ water at 413 K (Figure 3). $(SX^+)@SO_3H$ exhibited a better catalytic activity, with 81% cellobiose conversion and a 75% glucose yield, compared to CB (53% conversion and 50% glucose yield), due to the presence of a higher number of active sites available at the support's surface (determined by EDX, Figure S3, Supporting Information). For comparison, references were also performed without catalyst (blank run) and with pristine activated carbon (SX^+ blank run) and carbon black (CB blank run) under the same reaction conditions (Figure 3). As expected, a very low conversion ($< \approx 22\%$) and glucose yield ($< \approx 13\%$) were found in all three cases, with the blank giving the lowest conversion (9.4%). In the case of SX^+ blank run, a slight increment in the conversion and yield was observed in virtue of the weak Brønsted acid sites present at the surface of the pristine support due to surface O-groups (0.04 mmol g^{-1}, Table 5). Finally, negligible traces of fructose

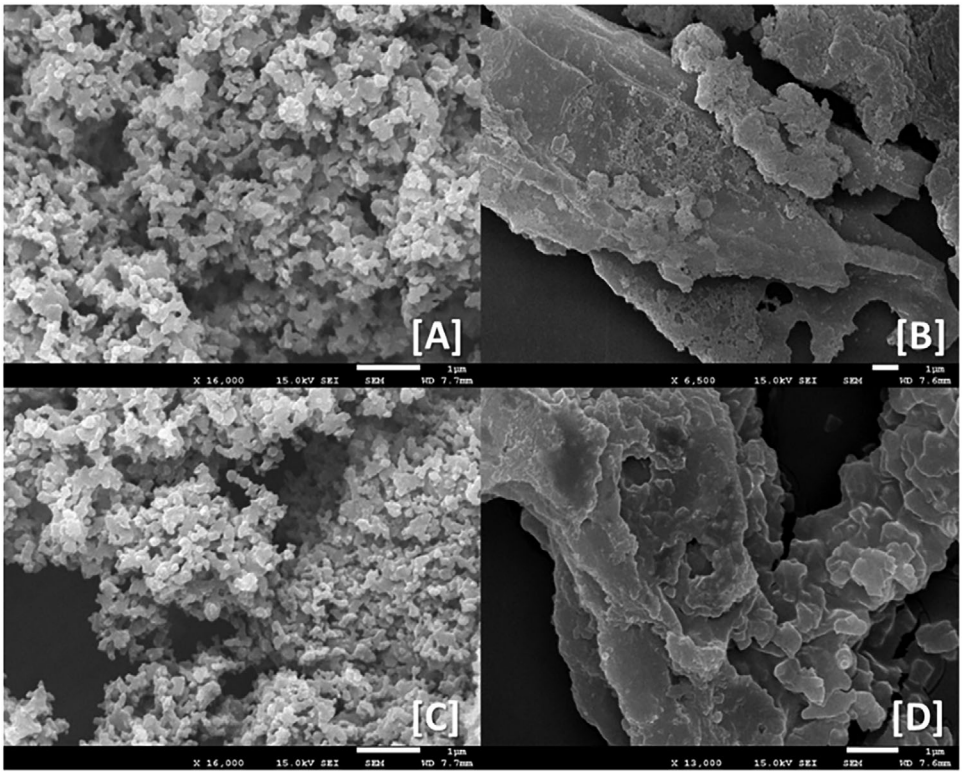

Figure 2. SEM images of carbon black (CB) (A) and activated carbon (SX^+) (B) before sulfonization, and carbon black (C) and activated carbon (D) after sulfonization. Different magnifications (hence scale bars) were applied to image the two substrates due to the difference in particles size.

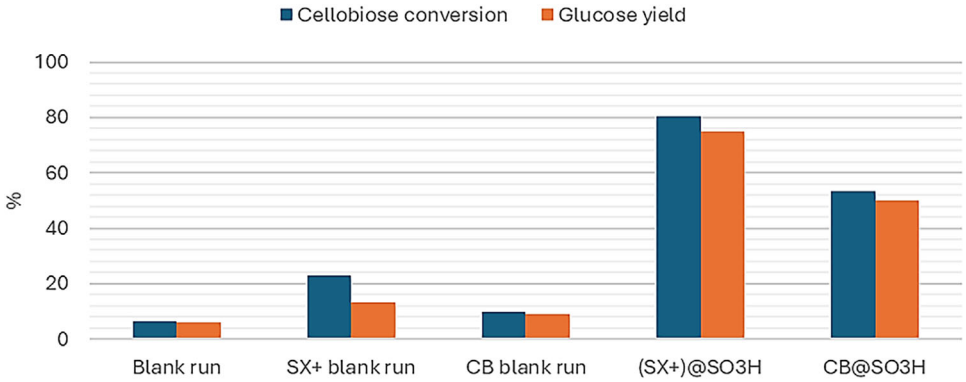

Figure 3. Conversion of cellobiose into D-glucose in a monophasic environment (mQ water) at 413 K.

were detected for all the tests performed (Figure S1, Supporting Information). As expected, the reaction did not proceed forward to 5-HMF formation due to the absence of Lewis acidic centers in these materials.

The next step in the functionalization of the carbon substrates was taken by developing an optimized methodology for the formation of a discontinuous oxide layer at their surface in coexistence with the sulfonic groups. Displaying no acidity and being not suitable for the grafting of sulfonic moieties (Figures S2, S3, and S11, Supporting Information, respectively), silica was chosen as a simplified reference oxide for this preliminary study. Starting from a continuous layer, which appears very homogeneous in the case of CB (Figure 4A) and more irregular in the case of SX^+ (Figure 4B), the amounts of precursors introduced were

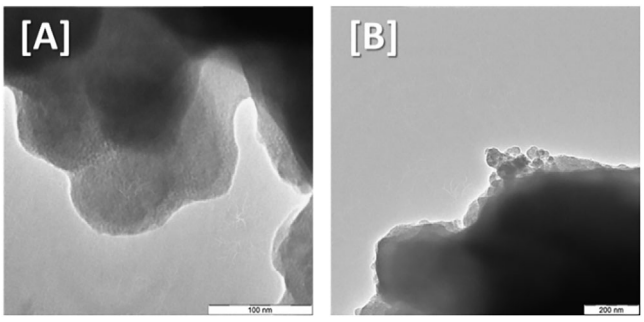

Figure 4. TEM images of carbon black (A) and activated carbon (B) coated with a continuous silica layer. Different magnifications were applied to image the two substrates due to the difference in their particles size.

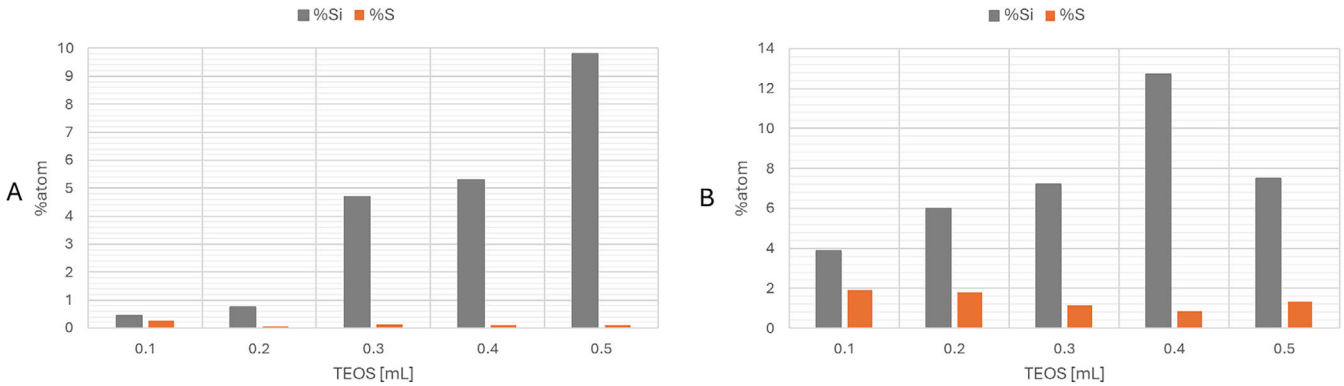

Figure 5. Si and S composition profiles determined by EDX elemental mapping in function of the adjusted amount of TEOS introduced (see Table 1 for details) for both CB (A) and SX^+ (B) decorated with silica patches and sulfonic groups.

Table 2. EDX mapping of the main elements of interest in alumino-silica decorated carbon samples; qualification reported in % atoms of the elements.

Entry	%Si	%Al	Al/Si	%S
I0@BATEOS	3.92	3.89	0.99	—
I0@BATEOS/SO_3H	3.38	1.54	0.46	0.35
I4@BATEOS	1.64	1.72	1.05	—
I4@BATEOS/SO_3H	1.41	0.85	0.60	0.82
I0@BATEOS/SO_3H inverse	4.77	4.27	0.89	0.39
I4@BATEOS/SO_3H inverse	1.49	1.55	1.04	0.87

modified by decreasing their quantities while maintaining their optimized relative molar ratio[30] to produce five different coated samples for each carbon type by growing the oxide layer first and grafting the benzyl sulfonic moieties in a second step. The prepared materials were named T0@SiO_2/SO_3H, T1@SiO_2/SO_3H, T2@SiO_2/SO_3H, T3@SiO_2/SO_3H, and T4@SiO_2/SO_3H, and their elemental compositions are listed in Table 2 below, as determined by EDX mapping.

As expected, by reducing the amounts of reactants, the extent of the oxide layer diminished and more free space was made available at the carbon surface for the introduction of the sulfonic moieties. Therefore, as shown in Figure 5 and Figure S4 (Supporting Information), by going from T0@SiO_2/SO_3H, where an average of 9.81% Si and 0.097% S was found on CB (similarly, 7.52% Si and 1.33 % S in the case of SX^+) when the highest amount of TEOS precursor was introduced, to T4@SiO_2/SO_3H, with an average of 0.44% Si and 0.27% S grafted on CB (3.89% Si and 1.89% S on SX^+), where the lowest amount of TEOS precursor was introduced, an inverse relationship can be observed between the two elements in terms of composition (Figure 5). In the case of activated carbon, because of the more irregular morphology of the support's particles, a small anomaly was observed for T1@SiO_2/SO_3H, where S is decreased to 0.86% in favor of a 12.7% of Si, and similarly for T2@SiO_2/SO_3H, where the 1.13% found for sulfur is again lower than the value reported for T0@SiO_2/SO_3H. In any case, the general expected elemental trend was not affected (Figure 5). To exclude any modification in sulfur's speciation, XPS measurements were performed. The S2p peak (reference peak for sulfonic groups) was found at a binding energy of 168 eV for all the samples analyzed (Figure S5, Supporting Information), confirming the sulfonic nature of the introduced moieties.

Overall, the best results in terms of growth of a discontinuous oxide layer at the surface in coexistence with benzyl sulfonic groups were attained with SX^+ as substrate. Particularly, the elemental maps acquired by EDX for this support in the case of T4@SiO_2/SO_3H (Figure 6) clearly show the bifunctional nature attained, with the appearance of metal oxide patches located at the support's surface (Si, O), in coexistence with sulfur (S), this latter element preferentially grafted to the carbonaceous surface. Therefore, in virtue of the properties displayed, the substrate of choice for the development of a bifunctional active acid system was SX^+.

3.2. Synthesis and Characterization of Carbon-Based (SX^+) Bifunctional Acid Catalysts

Bifunctional Brønsted/Lewis acid catalysts were successfully obtained by using a single molecular precursor [(sec-BuO)$_2$AlOSi(OEt)$_3$] (BATEOS), presenting both Al and Si centers in close contact and with a 1 to 1 ratio.[37] This compound offers a perfect solution for overcoming the difference in hydrolysis/condensation rates otherwise encountered when employing single metal alkoxides separately, possibly leading to a final inhomogeneous composition of the alumino-silica framework.[31] Additionally, this precursor will provide the necessary Lewis acidity needed in combination with Brønsted acid sites to facilitate the catalytic transformation of 5-HMF from cellobiose. Considering what has been observed and concluded in our preliminary study concerning the attainment of a patchy oxide and sulfonic-grafted material, catalysts I0@BATEOS/SO_3H and I4@BATEOS/SO_3H were synthesized from SX^+. The compositional difference between the two systems lies in the number of Brønsted and Lewis acid sites introduced.

The morphology and composition of the obtained catalysts I0@BATEOS/SO_3H and I4@BATEOS/SO_3H, of their monofunctional reference solids I0@BATEOS and I4@BATEOS, and their inversed counterparts (I0@BATEOS/SO_3H inverse and I4@BATEOS/SO_3H

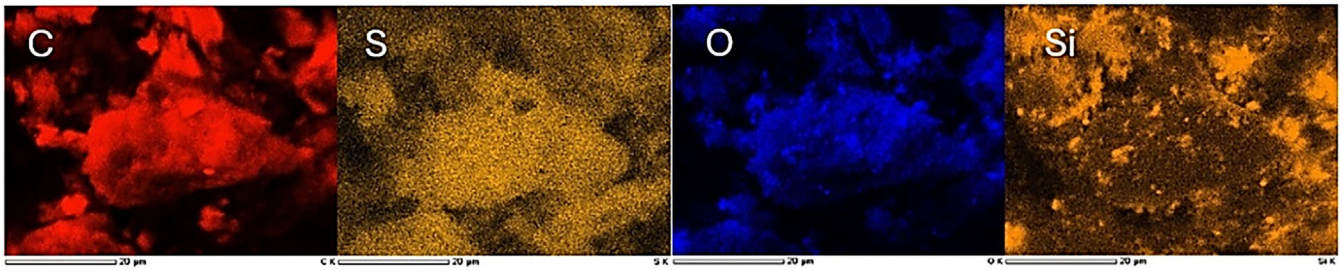

Figure 6. EDX maps of the main elements of interest (C, S, O, and Si) with SX^+ as substrate: trial T4@SiO_2/SO_3H.

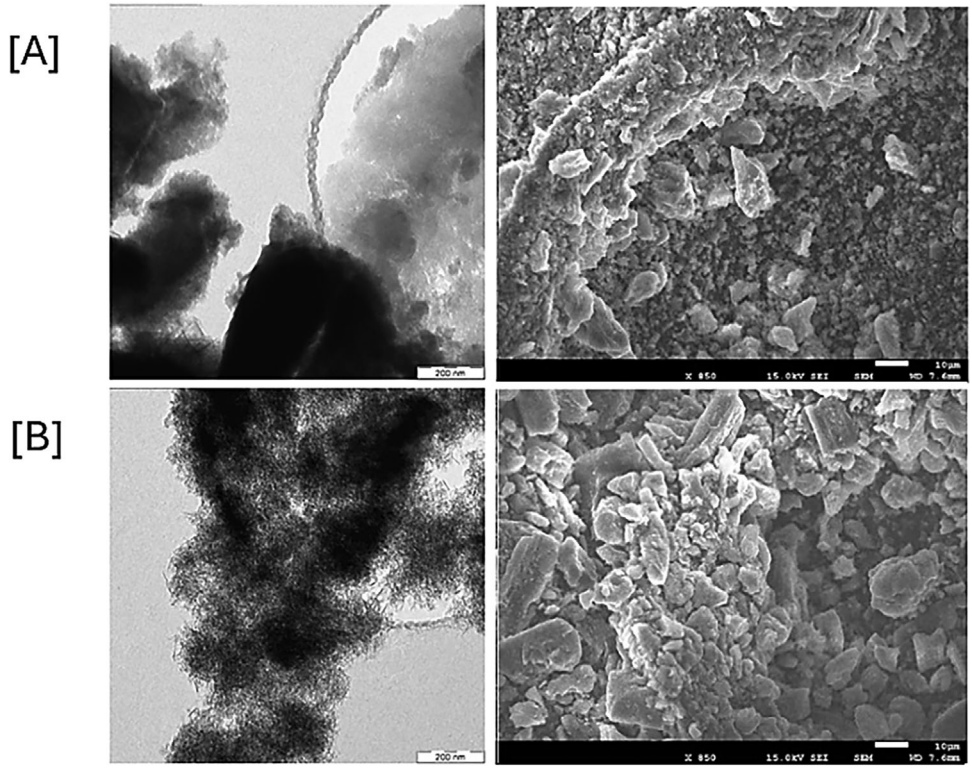

Figure 7. TEM and SEM images of (A) I0@BATEOS/SO_3H and (B) I4@BATEOS/SO_3H.

inverse) have been studied through electron microscopy, EDX probing, and XPS analyses. The inversed counterparts are samples prepared by reversing the steps of the applied methodology, performing the diazonium coupling method before the introduction of the metal-oxide patches.

The SEM images (Figure 7) showed the globular texture expected from an oxide surface. This characteristic morphology was observed to become less prominent when a lower amount of BATEOS was introduced, as seen in the case of I4@BATEOS/SO_3H. Additionally, TEM findings revealed a compact oxide layer at the surface of I0@BATEOS/SO_3H (Figure 7A), while a less dense and more dendritic appearance was remarked when the amount of precursor is reduced at its minimum (I4@BATEOS/SO_3H, Figure 7B).

In order to confirm that the composition of the aluminosilicate layer is homogeneous, EDX analyses were performed on all samples. As shown in Table 2, an aluminum/silicon ratio equal to 1 was found for both monofunctional cases, with 3.92% Si and 3.89% Al determined for I0@BATEOS and 1.64% Si and 1.72% Al found for I4@BATEOS. A similar Al/Si ratio was observed for the inversed counterparts, with 4.77 % Si and 4.27 % Al for I0@BATEOS/SO_3H inverse, and 1.49% Si and 1.55% Al for I4@BATEOS/SO_3H inverse. These findings demonstrate how the use of BATEOS as a single molecular precursor allows the deposition of a homogeneous bimetallic oxide layer.

In the case of the regular methodology, where the discontinuous metal-oxide layer is grown before performing the sulfonic functionalization (Table 2), the aluminum content is almost halved after the grafting of SO_3H moieties. In addition, a small loss of silicon was also detected, however expected and known not to be detrimental to the properties of the attained materials.[30] Aluminum oxide materials are known to be sensitive to the pH, and dissolve when interacting with acid or basic solutions. The resulting Al speciation is especially complex.[38] Given that Al^{3+} exists at pH $<$ 4, the environment provided by the diazonium coupling method employed (pH $\cong$ 2.5) has

Table 3. XPS results for the main elements of interest for the bifunctional catalyst I4 at each step of its synthesis by following an inverse methodology; quantification reported in % atoms.

Entry	%Si	%Al	%S
$(SX^+)@SO_3H$	–	–	3.61
$I4@SO_3H$/Cl inverse	–	–	3.25
$I4@SO_3H$/APTES inverse	2.17	–	2.94
I4@BATEOS/SO_3H inverse	15.11	3.97	2.08
I4@BATEOS/SO_3H	10.29	5.32	2.16

facilitated the lixiviation of some Al centers in the solution. By opposition, Al depletion was not detected when the catalysts were synthesized by the inversed methodology (Table 2). In this case, the oxide is grown subsequently to the grafting of sulfonic groups, thus preventing the layer from entering in direct contact with the acid environment.

Finally, EDX mappings revealed how sulfur (S) is preferentially grafted to the carbonaceous substrate while aluminum (Al) and silicon (Si) are co-located at the surface of the support in the form of metal-oxide patches (Figures S6 and S7, Supporting Information). It is also interesting to notice how the overall sulfur content detected for the bifunctional catalysts and their respective inverted counterparts is comparable (Table 2), where 0.35% S was reported for I0@BATEOS/SO_3H, and 0.39% S was found for I0@BATEOS/SO_3H inverse. Similarly, 0.82% S was observed for I4@BATEOS/SO_3H against a 0.87% S in the case of I4@BATEOS/SO_3H inverse. The EDX findings discussed in terms of homogeneous composition of the oxide patches (Si/Al ratio equal to 1, Table 2), and loss of aluminum centers after grafting of sulfonic moieties were also proven by elemental microanalyses and quantitative ICP (Figure S8, Supporting Information).

To corroborate the observations done so far and explore more the superficial elemental composition of the very same materials, XPS analyses have also been performed. The results confirmed the previously remarked loss of aluminum centers if sulfonization is done as a second step and highlighted an enrichment in Si at the surface compared to bulk for the patches (Table 3; Figure S8, Supporting Information). In order to exclude the possibility that the conditions required for the growth of the metal oxide patches could have been detrimental to the already grafted sulfonic moieties, XPS was also applied to study the speciation of sulfur in relation to the reverse synthetic pathway. The S 2p peak (reference peak for sulfonic groups) was found at a binding energy of 168 eV for all the samples analyzed, thus confirming the presence of a sulfonic contribution (Figure S10, Supporting Information). A peak at 155 eV indicative of the presence of —SH and S—S species was also found in the cases of $I4@SO_3H$/APTES inverse, I4@BATEOS/SO_3H inverse, and I4@BATEOS/SO_3H obtained from the regular methodology (Figure S10, Supporting Information). Furthermore, the sulfur content was also preserved by going from $(SX^+)@SO_3H$ (3.61% S, Table 3) to the carbon-APTES intermediate (2.94% S, Table 3) through the chlorinated stage (3.25% S, Table 3), taking I4@BATEOS/SO_3H inverse as a representative case. Finally, the attained bifunctional catalyst I4@BATEOS/SO_3H inverse showed a small decrement in the sulfur content if compared to the pristine sulfonated carbon $(SX^+)@SO_3H$, but with a 2.08% S, the value is highly comparable with the final 2.16% S reported for the same catalytic system synthesized via the regular methodology (I4@BATEOS/SO_3H, Table 3).

3.3. Application: Direct Conversion of Cellobiose into 5-HMF

The four bifunctional Brønsted/Lewis acid catalysts synthesized, namely I0@BATEOS/SO_3H, I4@BATEOS/SO_3H, I0@BATEOS/SO_3H inverse, and I4@BATEOS/SO_3H inverse, were tested for the conversion of cellobiose into 5-HMF over a 4 h reaction in a designed mixture of THF and mQ water, at the chosen temperature of 423 K. The obtained results (Figure 8) showed how the catalysts synthesized via the direct methodology were far more active in comparison to their inversed counterparts. I0@BATEOS/SO_3H and I4@BATEOS/SO_3H have achieved a conversion of 80% and 92%, respectively, with a yield of 7% and 12% in 5-HMF (and corresponding selectivity equal to 9% and 12%). On the other hand, I0@BATEOS/SO_3H inverse and I4@BATEOS/SO_3H inverse (both yielding ≈1% of 5-HMF, Figure 8) were found to be almost non-active. These last results are a direct consequence of the methodology applied, where the discontinuous oxide layer was grown after grafting the sulfonic moieties at the surface of the substrate. This has led to an isolation of some of the Brønsted sites by their coating with the discontinuous oxide, preventing their optimal interaction with the available cellobiose to be converted. Therefore, even though an inversed synthetic pathway is suitable for preserving the pH-sensitive system from Al leaching (leading to the loss of Lewis active centers), the observed performance makes these catalysts not relevant for a further development of the catalytic application.

The powders recovered after one catalytic test (R-I0@BATEOS/SO_3H, R-I4@BATEOS/SO_3H, R-I0@BATEOS/SO_3H inverse, and R-I4@BATEOS/SO_3H inverse) have been studied through electron microscopy and EDX probing to verify if any compositional change was induced in the materials in presence of the reaction mixture when compared to the freshly synthesized catalysts (Table 2). Considering the data obtained (Table 4), no modifications were brought about to the global elemental composition when R-I0@BATEOS/SO_3H, R-I4@BATEOS/SO_3H, R-I0@BATEOS/SO_3H inverse, and R-I4@BATEOS/SO_3H inverse were compared to the fresh catalysts (Table 2), and no important alterations in the global S content were detected, demonstrating that the patchy coatings and sulfonic groups are stable in the conditions chosen for the reaction.

A subsequent set of catalytic tests was performed to compare the activity of the bifunctional systems with that of the corresponding monofunctional solids I0@BATEOS and I4@BATEOS (Lewis acidity as the main contribution) in combination with $(SX^+)@SO_3H$ (Brønsted acidity provider). To have a number of active sites that is comparable with that of the bifunctional system of reference, the ratio between moles of active sites and moles of converted feedstock were calculated knowing the exact elemental composition of the materials involved (Figure

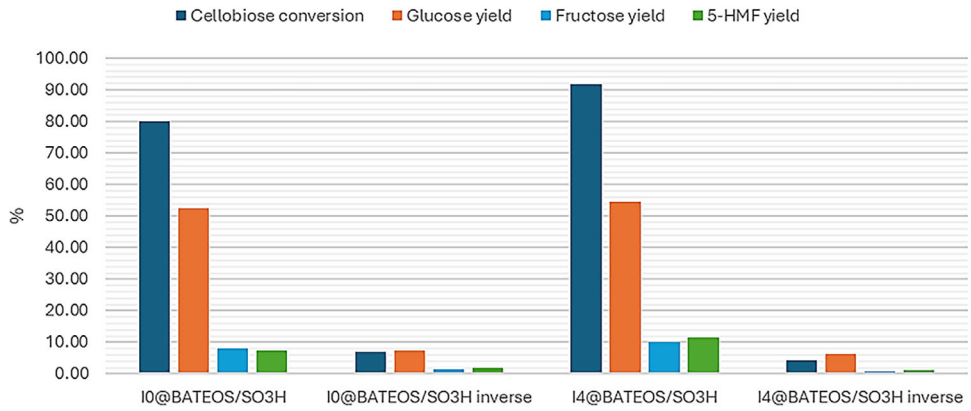

Figure 8. Conversion of cellobiose into 5-HMF; in THF:mQ water system, 4 h, 423 K; catalyst tested: I0@BATEOS/SO_3H, I0@BATEOS/SO_3H inverse, I4@BATEOS/SO_3H, and I4@BATEOS/SO_3H inverse.

Table 4. EDX mapping of the main elements of interest in alumino-silica decorated carbon samples recovered after one catalytic test; qualification reported in %atoms of the elements.

Entry	%Si	%Al	%S
R-I0@BATEOS/SO_3H	3.07	1.38	0.29
R-I4@BATEOS/SO_3H	1.51	0.79	0.63
R-I0@BATEOS/SO_3H inverse	2.72	2.50	0.20
R-I4@BATEOS/SO_3H inverse	1.47	1.64	0.66

S8, Supporting Information) and maintained for the combined monofunctional materials introduced (Figure S10, Supporting Information).

A 68% conversion of cellobiose was found for the monofunctional mixture I0@BATEOS & (SX^+)@SO_3H, accompanied by a 4.5% yield and a 6.6% selectivity for 5-HMF. As for I4@BATEOS & (SX^+)@SO_3H, a better result was observed in comparison, leading to a 6% 5-HMF yield (and a 7.3% selectivity) out of a 84% conversion of the original feedstock (Figure 9). In both cases, the mixture of monofunctional catalysts provided a slightly better contribution to the isomerization step when compared to their respective bifunctional analogues. Indeed, 9.93% of fructose (15% selectivity) was obtained with I0@BATEOS & (SX^+)@SO_3H, while slightly less was instead found with I0@BATEOS/SO_3H (8.16% fructose accompanied by a 10 % selectivity, Figure 9). Similarly, I4@BATEOS & (SX^+)@SO_3H resulted in almost 12% fructose (13% selectivity) out of a 60% glucose yield, whereas its bifunctional counterpart only reached 10% fructose (11% selectivity) out of a 55% glucose yield. The observed trends could be explained by considering how, in the case of I0@BATEOS and I4@BATEOS monofunctional catalysts, the aluminum centers introduced, responsible for the Lewis contribution, were globally preserved (Table 2), given that the sulfonization step, known to be destabilizing the oxide framework due to the low pH reached (§3.2), was not performed on these materials. Nevertheless, from a global perspective, in terms of conversion and 5-HMF yield, the bifunctional systems I0@BATEOS/SO_3H and I4@BATEOS/SO_3H were found to be more active than their monofunctional analogues (Figure 9), proving that a synergy was brought about by the combination of the two acid sites in close proximity onto the same substrate.

To better highlight the efficiency of the monofunctional systems I0@BATEOS and I4@BATEOS in mediating the isomerization of glucose into fructose, and that of the bifunctional catalysts I0@BATEOS/SO_3H and I4@BATEOS/SO_3H in facilitating fructose dehydration to 5-HMF, an additional set of catalytic tests was performed for the selected intermediate steps (Figure S11,

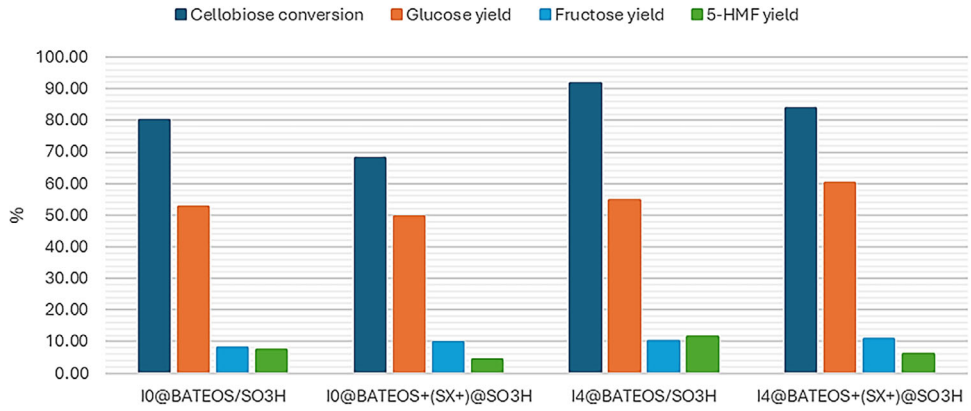

Figure 9. Conversion of cellobiose into 5-HMF; THF:mQ water system, 423 K; comparison between I0 and I4 bifunctional systems and their monofunctional counterparts I0@BATEOS and I4@BATEOS.

Table 5. Total acidity and textural properties of the best performing catalysts; BET specific surface area (S_{BET}) and pore volume (V_p) determined via the Barrett-Joyner-Halenda model.

Entry	S_{BET} ($m^2\ g^{-1}$)	V_p ($cm^3\ g^{-1}$)	Pore Size (Å)	Total Acidity[a] (mmol g^{-1})
(SX^+) Starting carbon	913	0.34	17.6	0.04
(SX^+)@SO_3H	124	0.17	31.7	1.33
I0@BATEOS/SO_3H	187	0.14	26.6	1.66
I4@BATEOS/SO_3H	89	0.12	45.8	1.25

[a] Boehm back titration.

Supporting Information). The advantage brought by combining the two acidic functions in a single catalyst instead of providing them as a mixture of monofunctional sources was also further corroborated. The catalytic conditions applied were maintained as before for the whole cascade reaction.

In the case of glucose to fructose isomerization, both catalysts were found to be highly selective for the targeted step (≈99% for I0@BATEOS and ≈97% achieved by I4@BATEOS) and more active than the control blank run (Figure S11, Supporting Information), proving once again the necessity of introducing Lewis acid sites to promote such a step. A better performance was observed in the case of catalyst I0@BATEOS in virtue of the higher number of Lewis active sites introduced, with 20.3% glucose conversion leading to a 20.1% fructose yield. Nevertheless, the absence of sulfonic moieties (Brønsted acid sites) is resulting in low 5-HMF yields for both monofunctional catalysts.

When starting from fructose dehydration, complications such as potential poisoning of the available active sites were avoided, easing the production of 5-HMF if compared to the results obtained through a cascade process (Figure 9). The catalytic nature of both materials was also confirmed by their prominent activity if compared to the results found for the control blank run. In fact, 41% 5-HMF yield (69% selectivity) was observed in the case of I4@BATEOS/SO_3H, whereas I0@BATEOS/SO_3H resulted in 14% of the targeted molecule. The enhanced 5-HMF yield observed for catalysts I4@BATEOS/SO_3H is ascribable to the higher density of sulfonic moieties introduced in this case.

The textural properties of the best performing materials I0@BATEOS/SO_3H and I4@BATEOS/SO_3H were then investigated to link these features to the observed catalytic activity. Table 5 below reports the main findings in terms of surface area and porosity for the systems studied.

For both materials, a type IV isotherm with N_2 hysteresis loop was observed, together with monomodal pore size distributions (Figure 10), indicating the mesoporous nature of the synthesized catalysts.[39]

A decrement in the surface area measured was observed when going from the pristine SX^+ carbon substrate (913 $m^2\ g^{-1}$, Table 5) to its sulfonated counterpart (SX^+)@SO_3H (124 $m^2\ g^{-1}$, Table 5) due to the occlusion of preexisting micro and nanopores by functionalization. When considering catalyst I0@BATEOS/SO_3H, an increment in the specific surface area (187 $m^2\ g^{-1}$, Table 5) was instead remarked in comparison to (SX^+)@SO_3H, thanks to the mesoporous nature of the discontinuous metal oxide layer introduced. By contrast, an unexpected decrease in S_{BET} was found for I4@BATEOS/SO_3H (89 $m^2\ g^{-1}$, Table 5), where the deposited Al-Si could have possibly blocked most of the smallest pores without forming much overlayer in reason of the lower amounts of starting reagents introduced for the growth of the mixed oxide itself, resulting in the increment of the proportion of larger mesopores (average pore size = 45.8 Å, Table 5). This latter feature could have positively impacted the catalytic performance observed, where wider pores might have facilitated the accommodation of the bulky sugary precursors in proximity to the available active sites, easing their conversion. A smaller pore size of 26.6 Å, (Table 5) was instead found for I0@BATEOS/SO_3H. These latter observations were in good accordance with the TEM investigation carried out (Figure 7), revealing a more compact oxide framework for I0@BATEOS/SO_3H and a less dense structure in the case of I4@BATEOS/SO_3H.

In parallel, the total acidity was determined through Boehm back titration.[32,33] It is important to note that the pH sensitivity evidenced for the aluminosilicate framework in use might have possibly influenced the global detection of acid sites due to the leaching of Al species in solution, so these numbers have to be taken with caution. Catalyst I0@BATEOS/SO_3H displayed the highest total acidity (1.66 mmol g^{-1}, Table 5), whereas I4@BATEOS/SO_3H achieved a lower value of 1.25 mmol g^{-1}. Nevertheless, I4@BATEOS/SO_3H was found to be the most active system (Figure 8).

To better understand the acidic properties of the two solids in terms of Bronsted versus Lewis acidity and highlight potential differences arising from their distinct morphologies, a solid-state NMR (ssNMR) analysis was carried out. It is well known that probe molecules such as trimethylphosphine (TMP), trimethylphosphine oxide (TMPO), pyridine (Py), acetonitrile, and others, analyzed via ssNMR, can provide valuable insights into the nature of acidic sites (Brønsted or Lewis) and their relative strength.[34] In particular, specific signals corresponding to TMP interactions with Brønsted or Lewis acid sites can be observed via ^{31}P ssNMR. TMP was selected because of its broad chemical shift range, which allows distinguishing clearly Brønsted and Lewis signals, as well as Lewis acid sites with different strengths. Furthermore, ^{31}P nucleus has a 100% natural abundance, making isotopic enrichment unnecessary. It is important to mention that before conducting the analysis, it is essential to ensure that the material is properly dehydrated. For this study, the carbon-based material was mixed with pristine silica, a nonacidic solid (Figure S16, Supporting Information; Figure 11). When TMP interacts with Brønsted acid sites, signals typically appear in the region between −2 and −5 ppm. In contrast, interactions with Lewis acid sites result in contributions in the range from −20 to −60 ppm.[41] However, it is important to note that TMP is highly susceptible to oxidation. In the presence of small amounts of oxygen, TMP can oxidize to TMPO, necessitating meticulous control of the experimental setup.[34]

Figure 11 presents the spectra of the I0@BATEOS/SO_3H and I4@BATEOS/SO_3H samples acquired at a spinning speed of 8 kHz. A comparison reveals three main signals along with their respective spinning sidebands.

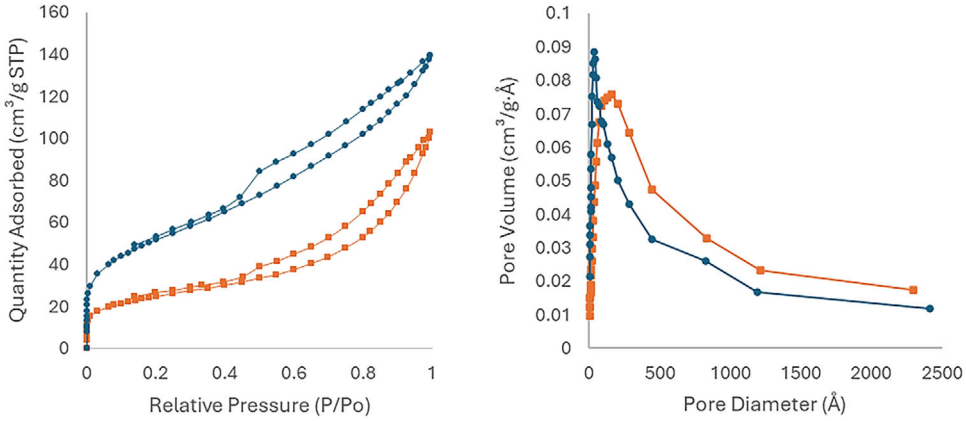

Figure 10. Nitrogen adsorption-desorption isotherms at 77 K (left) and pore size distribution obtained by the Barrett-Joyner-Halenda method (right) for I0@BATEOS/SO_3H (orange) and I4@BATEOS/SO_3H (blue).

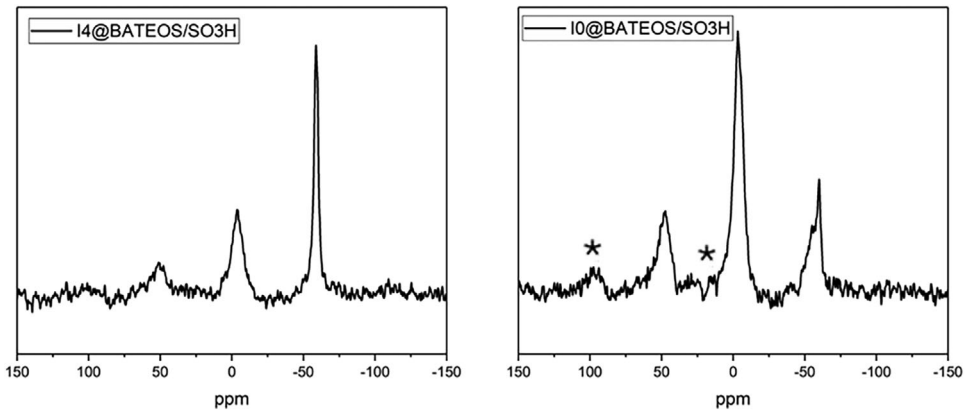

Figure 11. ^{31}P ssNMR-TMP analysis on catalysts I4@BATEOS/SO_3H (left) and I0@BATEOS/SO_3H (right). Asterisks indicate the spinning sidebands.

The signal centered ≈ −4 ppm corresponds to TMP bonded to Brønsted active sites, while the one centered at −58 ppm is associated with TMP interacting with Lewis acid sites.[34,41] Specifically, in the case of I0@BATEOS/SO_3H, the peak at −58 ppm reflects weak Lewis acid sites interacting with TMP and includes a minor contribution from the physisorbed probe molecule.[41,42] In the case of I4@BATEOS/SO_3H, this signal can be exclusively assigned to weak Lewis acid sites interacting with TMP.[42] A stacked version of the two spectra is reported in supporting information (Figure S17, Supporting Information). As previously mentioned, TMP is highly susceptible to oxidation. The signal at ≈50 ppm can be reasonably attributed to a fraction of TMP oxidized to TMPO still bonded to Lewis acid sites.[43]

In summary, the analysis clearly indicated the presence of both Brønsted and Lewis acidity on the studied materials. Moreover, I4@BATEOS/SO_3H displayed a higher quantity of Lewis active sites compared to I0@BATEOS/SO_3H, feature that has definitely impacted the catalytic results by facilitating the isomerization step (Figure 8). Due to the high reactivity of the functionalized materials toward TMP, it was impossible to prevent oxidation phenomena. Therefore, only qualitative analyses were performed on catalysts I4@BATEOS/SO_3H and I0@BATEOS/SO_3H.

Provided that the best catalytic performance was observed for I4@BATEOS/SO_3H in virtue of the higher amount of Brønsted and Lewis groups introduced (Figure S8, Supporting Information; Figure 11, respectively) when compared to I0@BATEOS/SO_3H, the system was kinetically studied over 23 h (biphasic solvent mixture, 423 K) to better understand its potential. An interesting correlation was observed between cellobiose conversion, glucose and fructose consumption, and 5-HMF production. Cellobiose reached its maximal conversion (96%) after 8 h (Figure 12), whereas glucose (in orange) was consumed over time favoring the formation of fructose (11% yield achieved after 8 h, Figure 12). Fructose was then mainly consumed to produce 5-HMF (in green), with a satisfactory 37% yield (accompanied by a selectivity of the 38%) after 23 h. Negligible traces of other sugary compounds, possibly side-products, have been found (Figure S12, Supporting Information), proving the high selectivity of catalyst I4@BATEOS/SO_3H for the process of valorization of cellobiose into 5-HMF. Moreover, by comparing the conversion (cellobiose) and yield (5-HMF) attained after 4 h, the kinetic study (Figure 12) is in good accordance with our previous catalytic test, carried out with substrate I4@BATEOS/SO_3H from a different batch under the exact same conditions (Figure 8). In fact, almost 92% of converted cellobiose and 12% of 5-HMF were detected after 4 h in both cases. Therefore, a satisfactory reproducibility of the whole methodology, from synthesis to catalytic activity testing, was also achieved.

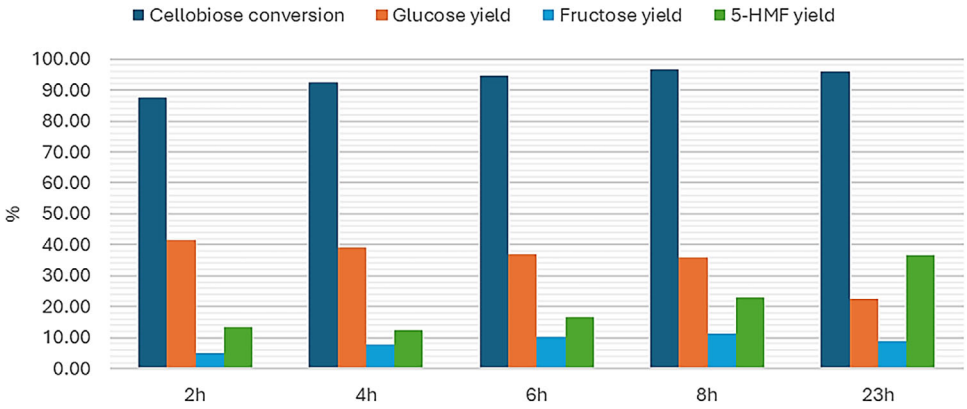

Figure 12. Conversion of cellobiose into 5-HMF; THF:mQ water system, 423 K; kinetic study with catalyst I4@BATEOS/SO_3H over 23 h.

Table 6. Catalytic results for a series of selected blanks tested for the conversion of cellobiose into glucose, fructose and 5-HMF; biphasic system (THF:mQ water), 423 K, 4 h.

Entry	Cellobiose Conversion (%)	Glucose Yield (%)	Fructose Yield (%)	5-HMF Yield (%)
Blank	9.4	9.0	1.0	1.0
SX^+	24.2	22	0.81	0.49
$(SX^+)@SO_3H$	99	32	34	7.7
$T0@SiO_2$	15	16	0.37	2.546
$T0@SiO_2/SO_3H$	26	15	3.4	0.83
$T4@SiO_2$	20	16	1.1	0.36
$T4@SiO_2/SO_3H$	94	24	1.1	3.81
I0@BATEOS	9.3	7.0	1.8	1.5
I4@BATEOS	3.1	5.0	0.78	0.82
SiO_2 pure oxide	20	16	5.0	0.02
Al-Si pure mixed oxide	18	8.6	3.4	1.6

The reaction kinetics of cellobiose conversion at 150 °C was evaluated using a simple power-law model which indicated that cellobiose decomposition followed first-order kinetics with a rate constant of 0.49 h^{-1} and an R^2 value of 0.98. These results are consistent with the data reported by previous studies.[45,46] The detailed analysis including 5-HMF productivity is provided in Figure S13 (Supporting Information).

Finally, a set of selected blanks was tested to corroborate the catalytic study and provide a better insight into the substrate-functionalities relationship (Table 6). The synergy between support and introduced sulfonic moieties was evident when comparing catalyst $(SX^+)@SO_3H$ and its striking 99% conversion (Table 6), achieved thanks to the Brønsted acidity provided by the $-SO_3H$ groups grafted, with the bare SX^+ substrate (24% conversion, Table 6) and the 9.4% conversion reported for the blank run (no catalyst), this latter result being mainly promoted by the effect of temperature on the water-soluble dimer.

When silica oxide patches were introduced onto the carbon substrate in a proportion designed to outnumber the grafted Brønsted sites, as for $T0@SiO_2/SO_3H$, only 26% conversion was achieved (Table 6), resulting in an overall less active system in comparison to $T4@SiO_2/SO_3H$, where a larger portion of free surface remained available for the introduction of benzyl sulfonic moieties. 94% conversion was attained with $T4@SiO_2/SO_3H$, accompanied by a 24% glucose yield (Table 6), thus making the outstanding performance of this blank also comparable to the one of catalyst $(SX^+)@SO_3H$, logically in line with the similar amount of sulfonic moieties grafted (Figure 5; Figure S3, Supporting Information). Nevertheless, the absence of Lewis acidity in the silica patches is preventing the cascade reaction under study from proceeding further than the glucose intermediate. In the case of active aluminosilicate patches deposited on carbon without sulfonic groups (samples I0@BATEOS and I4@BATEOS), the lack of strong Brønsted sites is instead hindering an optimal conversion, resulting in almost nonactive materials and a thermally driven outcome. A slightly better performance was achieved with I0@BATEOS (9.3% conversion, 1.5% 5-HMF yield, Table 6), thanks to the higher amount of alumino-silica introduced, whereas only 3.1% conversion and ≈1% 5-HMF yield was obtained with I4@BATEOS. As a last step, by comparing the two pure oxides, a small Brønsted acid contribution from the silica, resulting in a conversion of almost 20% and a 16% glucose yield (Table 6) could be observed.

A higher 5-HMF yield (1.6%, Table 6) was instead found for the aluminosilicate oxide synthesized from BATEOS, thanks to the Brønsted-Lewis acidity introduced facilitating the isomerization of glucose into fructose, and finally, the conversion of the latter into the targeted molecule. Once again, the overall results were mostly thermally driven, pointing out the importance of providing both Brønsted and Lewis acid sites to catalytically control the whole cascade process from cellobiose to 5-HMF.

In the interest of an overall understanding of the catalytic results observed for the pure oxide blanks, their acidity was also investigated. Therefore, Py-FTIR and NH_3-TPD have been performed on both SiO_2 and the aluminosilicate pure oxides (Figures S14 and S15, Supporting Information). As expected, SiO_2 displayed no relevant acidity, despite the catalytic findings (Table 6). On the contrary, the aluminosilicate solid presented both types of acid sites, with a prevalence of Brønsted contribution leading to a L/B ratio of 0.15 (Figure S18, Supporting Information).

4. Conclusions and Perspectives

Bifunctional carbon-based Brønsted/Lewis acid catalysts have been successfully synthesized thanks to the development of a simple methodology involving the growth of aluminosilicate patches at the solid's surface and the subsequent grafting of benzyl sulfonic moieties on the uncoated areas. Overall, the bifunctional systems were found to be more active than their monofunctional or inverted analogues, proving that a synergy is apported by the combination of the two types of acidic sites in close proximity onto the same substrate, and that the order of applied synthetic steps is also influential upon the achievable properties. In addition, mesoporosity and the presence of both Brønsted and Lewis acid sites have been remarked as recurrent role-playing features for the optimal conversion of cellobiose into 5-HMF. Therefore, bifunctional catalyst I4@BATEOS/SO_3H, with an average pore size of 45.8 Å and a total acidity of 1.25 mmol g^{-1} accompanied by the presences of both Brønsted and Lewis acid sites, was found to be the best performing material, yielding 37% of 5-HMF out of a 96% conversion of the initial cellobiose feed when tested over 23 h at 423 K in a designed solvent mixture (THF:mQ water). Additionally, no significant side-products were observed after 23 h, indicative of the catalyst's high selectivity for the targeted molecules. Consequently, the attained results open the door to further developments by varying the nature of the introduced Lewis acid sites, their strengths and the relative ratio with respect to the Brønsted acid sites.

Acknowledgements

This project has received funding from the FWO and F.R.S.-FNRS (Belgium) under the Excellence of Science (EOS) program ("PHOSPORE" – EOS reference number: 40007504). The authors wish to thank Jean-François Statsyns for laboratory technical assistance and for performing the nitrogen physisorption analyses, and Pierre Eloy for the XPS training and help provided. Finally, the authors kindly acknowledge the University of Namur for carrying out the ^{31}P MAS ss-NMR analyses, and Mr. Oliver Garot for the technical support on the experimental set-up.

Conflict of Interests

The authors declare no conflict of interest.

Data Availability Statement

The data that support the findings of this study are available from the corresponding author upon reasonable request.

Keywords: 5-Hydroxymethylfurfural · Acidity · Aluminosilicates · Bifunctional catalysts · Carbon

[1] Y. Yao, S. Chen, M. Zhang, *Front. Chem.* **2022**, *10*, 880603.
[2] J. Sánchez, M. D. Curt, N. Robert, J. Fernández, *Biomass Resources* **2019**, 25–111.
[3] G. Shen, B. Andrioletti, Y. Queneau, *Curr. Opin. Green Sustain. Chem.* **2020**, *26*, 100384–100395.
[4] D. Haldar, M. K. Purkait, *Chemosphere* **2021**, *264*, 128523.
[5] W. Cao, J. Li, T. Martí-Rosselló, X. Zhang, *J. Energ. Inst.* **2019**, *92*, 1303–1312.
[6] A. M. Mansora, J. S. Lima, F. N. Anib, H. Hashima, W. S. Hoa, *Chem. Eng.* **2019**, *72*, 79–84.
[7] J. Yang, X. An, L. Liu, S. Tang, H. Cao, Q. Xu, H. Liu, *Carbohydr. Polym.* **2020**, *250*, 116881–116897.
[8] X. Huang, J. Ren, J.-Y. Ran, C.-L. Qin, Z.-Q. Yang, J.-P. Cao, *Fuel Process. Technol.* **2022**, *229*, 107175–107192.
[9] C. Thoma, J. Konnerth, W. Sailer-Kronlachner, P. Solt, T. Rosenau, H. W. G. van Herwijnen, *ChemSusChem* **2020**, *13*, 3544–3564.
[10] J. Ethiraj, D. Wagh, H. Manyar, *Energy Fuels* **2022**, *36*, 1189–1204.
[11] F. Menegazzo, E. Ghedini, M. Signoretto, *Molecules* **2018**, *23*, 2201;
[12] J.-P. Lange, *Nat. Catal.* **2021**, *4*, 186–192.
[13] S. Witzel, A. S. K. Hashmi, J. Xie, *Chem. Rev.* **2021**, *121*, 8868–8925.
[14] L. Yan, R. Ma, H. Wei, L. Li, B. Zou, Y. Xu, *Bioresour. Technol.* **2019**, *279*, 84–91.
[15] E. J. Güell, B. T. Maru, R. J. Chimentão, F. Gispert-Guirado, M. Constantí, F. Medina, *Biochem. Eng. J.* **2015**, *101*, 209–219.
[16] Y. Wang, A. Kiziltas, A. R. Drews, S. Tamrakar, P. Blanchard, T. R. Walsh, *Biomacromolecules* **2021**, *22*, 3884–3891.
[17] Z.-B. Huo, J.-K. Liu, G.-D. Yao, X. Zeng, J. Luo, F.-M. Jin, *Appl. Catal. A: Gen.* **2015**, *490*, 36–41.
[18] R. Sun, M. Zheng, J. Pang, X. Liu, J. Wang, X. Pan, A. Wang, X. Wang, T. Zhang, *ACS Catal.* **2016**, *6*, 191–201.
[19] X. Tan, P. Sudarsanam, J. Tan, A. Wang, H. Zhang, H.u Li, S. Yang, *J. Environ. Chem. Eng.* **2021**, *9*, 104719–104742.
[20] L. Cao, I. K. M. Yu, S. S. Chen, D. C. W. Tsang, L. Wang, X. Xiong, S. Zhang, Y. S. Ok, E. E. Kwon, H. Song, C. S. Poon, *Bioresour. Technol.* **2018**, *252*, 76–82.
[21] Y. Zhang, J. Wang, J. Wang, Y. Wang, M. Wang, H. Cui, F. Song, X. Sun, Y. Xie, W. Yi, *ChemistrySelect* **2019**, *4*, 5724–5731.
[22] M. Zuo, W. Che, W. Jia, Z. Zhou, X. Zeng, L. Lin, *Industrial Crops Products* **2023**, *194*, 116354.
[23] T. Yang, D. Chen, W. Li, H. Zhang, *Mol. Catal.* **2021**, *515*, 111920.
[24] N. Li, M. Xu, N. Wang, O. Shen, K. Wang, J. Zhou, *React. Kinet., Mech. Catal.* **2021**, *133*, 157–171.
[25] X. Zhang, D. Zhang, Z. Sun, L. Xue, X. Wang, Z. Jiang, *Appl. Catal., B* **2016**, *196*, 50–56.
[26] S. T. Pham, B.a M. Nguyen, G. H. Le, A. Sapi, S. Mutyala, I. Szenti, Z. Konya, T. A. Vu, *React. Kinet., Mech. Catal.* **2020**, *130*, 825–836.
[27] X. Xing, X. Shi, R. Hu, J. Guan, H. Gao, S. Xu, *Int. J. Biol. Macromol.* **2022**, *222*, 3014–3023.
[28] T. Zhang, H. Wei, R. Ling, Y. Jin, H. Xiao, W. Li, F. Seidi, *Microp. Mesop. Mater.* **2021**, *311*, 110717.
[29] S. Carlier, S. Hermans, *Front. Chem.* **2020**, *8*, 347.
[30] T. Haynes, O. Ersen, V. Dubois, D. Desmecht, K. Nakagawa, S. Hermans, *Appl. Catal., B* **2019**, *241*, 196–204.
[31] T. Haynes, T. D'hondt, A. L. Morritt, Y. Z. Khimyak, D. Desmecht, V. Dubois, S. Hermans, *ChemCatChem* **2019**, *11*, 4054–4063.
[32] S. L. Goertzen, K. D. Thériault, A. M. Oickle, A. C. Tarasuk, H. A. Andreas, *Carbon N. Y.* **2010**, *48*, 1252–1261.
[33] A. M. Oickle, S. L. Goertzen, K. R. Hopper, J. O. Abdalla, H. A. Andreas, *Carbon N. Y.* **2010**, *48*, 3313–3322.
[34] X. Yi, Y.-K. Peng, W. Chen, Z. Liu, A. Zheng, *Acc. Chem. Res.* **2021**, *54*, 2421–2433.
[35] M. Hunger, W. Wang, in (Eds: B.C. Gates, H. Knzinger), *Advances in Catalysis*, Academic Press, Cambridge, USA **2006**, pp. 149–225.
[36] D. R. Stellwagen, F. Van Der Klis, D. S. Van Es, K. P. De Jong, J. H. Bitter, *ChemSusChem* **2013**, *6*, 1668–1672.
[37] Y. Li, Q. Yang, J. Yang, C. Li, *Microporous Mesoporous Mater.* **2006**, *91*, 85–91.
[38] T. T. N. Nguyen, M. S. Lee, *Geosystem Engineering* **2019**, 1–7.
[39] M. Thommes, K. Kaneko, A. V. Neimark, J. P. Olivier, F. Rodriguez-Reinoso, J. Rouquerol, K. S. W. Sing, *Pure Appl. Chem.* **2015** *87*, 1051–1069.

[40] R. Tomer, P. Biswas, *New J. Chem.* **2020**, *44*, 20734-20750.
[41] A. Zheng, S.-B. Liu, F. Deng, *Chem. Rev.* **2017**, *117*, 12475–12531.
[42] X. Yi, H.-H. Ko, F. Deng, S.-B. Liu, A. Zheng, *Nat. Protoc.* **2020**, *15*, 3527–3555.
[43] C. Bornes, M. Fischer, J. A. Amelse, C. F. G. C. Geraldes, J. Rocha, L. Mafra, *J. Am. Chem. Soc.* **2021**, *143*, 13616–13623.
[44] E. Lam, J. H. T. Luong, *ACS Catal.* **2014**, *4*, 3393–3410.
[45] X. Liang, A. Montoya, B. S. Haynes, *Energy Fuels* **2017**, *31*, 2203–2216.
[46] N. V. Gromov, O. P. Taran, C. Aymonier, V. N. Parmon, *React. Kinet., Mech. Catal.* **2020**, *130*, 669–684.

Manuscript received: January 14, 2025
Revised manuscript received: March 13, 2025
Accepted manuscript online: March 25, 2025
Version of record online: April 28, 2025